Parametric Design, Manufacturing and Simulation of On-Demand Fixed Wing UAVs

Yash H. Chitale* and Cedric Y. Justin† and Dimitri N. Mavris‡
Aerospace Systems Design Laboratory, Atlanta, Georgia, USA

As the market for Unmanned Aerial Vehicles (UAVs) continues to expand, an unfulfilled need has been identified for tailor-made solutions leveraging an end-to-end process for the design and manufacture of the vehicle. The use of computer aided design combined with new manufacturing techniques allows small UAVs to be parametrically sized and quickly prototyped and deployed. This parametrization technique can be used throughout the entire design process to create optimized, attritable, on-demand solutions that can be adapted to evolving customer requirements. High-level requirements are mapped to quantitative design constraints and an automated process uses these constraints to design and manufacture a vehicle within a specified amount of time. The proposed framework is demonstrated with the generation of a fixed wing UAV solution for the detection and tracking of wildlife in remote areas. National Parks seek to prevent illegal poaching but often lack either the resources to monitor endangered animals, or the budget to purchase UAVs specially designed for wildlife tracking. First, mission requirements are identified and define a design space from which an optimal design point is selected. This design point sizes a UAV model, which is then optimized to minimize manufacturing time with the objective to yield a ready-to-fly solution within 48 hours. A flight simulation of the mission is then performed to ensure that the vehicle will fly as designed. Structural limitations of the UAV are accounted for and linked to parameters of the flight control algorithm to ensure that the UAV can safely fly its mission.

I. Introduction

In recent years, the use of UAVs in recreational, commercial, and military applications has greatly increased. Many general-purpose UAVs are available, but these off-the-shelf solutions may not be ideal for customers with unique and possibly evolving mission requirements that need tailor-made solutions. At the same time, custom UAV products can be prohibitively expensive, especially if the design requirements correspond to one-off missions. A low-cost, attritable, and on-demand solution that adapts to evolving requirements, but still leverages off-the-shelf components such as batteries, motors, and sensors is preferable.

One example of such a use case is a wildlife detection and tracking mission. Wildlife monitoring can be critical in detecting and preventing illegal poaching, which remains a major concern in many regions including parts of Africa. For instance, the critically endangered black rhino population has suffered a drastic decline in the wild (-96%) going from 65,000 animals in 1970 to just over 2,300 animals in 1993 [1]. Intense anti-poaching efforts since 1996 have allowed the species to slowly recover and the population has risen to over 5,630 animals in recent years. Poaching nonetheless remains a pressing issue with one rhino killed every 9 hours on average, adding up to 892 poached rhinos in 2018 [2]. Anti-poaching solutions run the gamut from preventive dehorning of rhinos [3] to 24-hour armed protection of animals [4]. These solutions come at a steep price that is barely affordable for national parks in developing countries. Many of these parks lack the resources to continuously monitor and protect endangered animals such as the black rhino of Fig. 1.

The ability to track rhinos and other endangered animals in real-time using aerial solutions could drastically improve the efficacy of anti-poaching measures. Such an aerial solution needs to be affordable in order to be deployed over large swaths of land by budget-constrained governmental and non-governmental agencies. At the same time, an aerial solution needs to be adaptable to enable the tracking of different types of animals and to respond appropriately to evolving poaching threats. While the UAV's endurance, range, speed, and cruise altitude may need to be adjusted to account for the changing location of animals, the payload may also need to be adjusted to account for the type of sensor to be carried

*Graduate Research Assistant, Aerospace Systems Design Laboratory, AIAA Member
†Research Engineer II, Aerospace Systems Design Laboratory, AIAA Member
‡S.P. Langley NIA Distinguished Regents Professor, Boeing Professor of Advanced Aerospace Analysis, Director of the Aerospace Systems Design Laboratory, AIAA Fellow

Fig. 1 Black rhino in Namibia's Etosha National Park

by the UAV (visible spectrum camera for day-time operations or infrared camera for night-time operations). The UAVs may also be needed for different types of missions ranging from wildlife geo-location to long-term wildlife monitoring, and detection and tracking of poaching activity [5]. Each of these missions theoretically yields a different set of requirements and therefore a different UAV solution. Designing a single vehicle able to carry out all these missions will likely yield an overly complex, heavy, and expensive solution. The authors hypothesize that these wide-ranging needs can be met using a combination of: a parameterized and automated design process that creates scalable and attritable UAV designs, in-situ manufacturing of a tailor-made UAV solution leveraging advances in additive manufacturing, and the use of affordable, readily available off-the-shelf components that can be rapidly integrated into the vehicle. The proposed design process can be broken down into several steps, as illustrated in Fig. 2. Connections between different steps highlight the coupled and interdependent nature of the process.

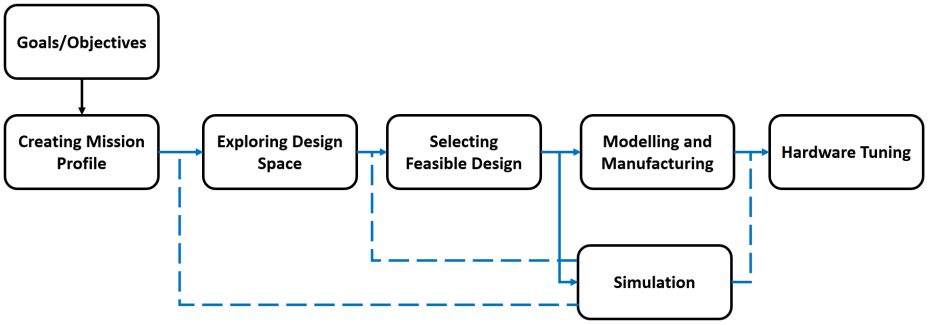

Fig. 2 Design process breakdown

First, high level mission objectives must be converted into a mission profile and the associated requirements that must be met by the UAV. This can include performance requirements such as cruise speed, ceiling altitude, endurance, range, maximum speed, ability to be hand-launched, as well as manufacturing requirements such as manufacturing time and manufacturing cost. Mission requirements can then be converted into engineering constraints that are used to define and explore the space of potential designs. Within this design space, an optimal design point is selected and its specifications are used to resize a baseline UAV configuration, to create a digital twin of the vehicle within a computer aided design environment, and to generate the appropriate manufacturing commands. A simulation environment is used in parallel to virtually fly the mission, to compare the performance of multiple designs, and to virtually test the final design. Results from the simulations are then used to fine-tune the model.

This paper focuses on several aspects of this proposed approach. A method for converting mission and manufacturing requirements into design constraints to enable the exploration of the design space is first proposed. An exploration of manufacturing time challenges is reviewed next and the authors propose the use of job-shop optimization algorithms to schedule the production of parts using additive manufacturing technologies. The identification of a design point

using off-the-shelf components and the sizing of the corresponding vehicle is then demonstrated. Finally, a low-fidelity simulation environment is developed and used to virtually test the performance of the vehicle and virtually test-fly the mission. The proposed approach is then applied using an animal movement dataset and the entire process is demonstrated. Throughout this research, the emphasis is on the parameterized nature of the process, which allows on-demand products to be created. A true on-demand solution that creates a product suited for a specific mission must include on-demand requirements analysis, design, and manufacture [6].

II. Design Space Exploration

The goal of the UAV design process is to obtain a well-defined design including the physical geometry, the set of off-the-shelf components needed, and some performance metrics that define how well the system performs the mission and achieves the various requirements. Converting requirements into constraints allows the designer to capture in a rigorous manner the limiting specifications that meet requirements [7]. These can include performance-oriented constraints, manufacturing constraints, and component selection constraints. These constraints are resolved into curves that specify Thrust to Weight (*T/W*) or Power to Weight (*P/W*) as a function of wing loading (*W/S*) [8]. A space of feasible designs where all constraints are met is then identified. A design point is selected next from the feasible design space and used to size a baseline vehicle. A constraint diagram that incorporates performance constraints, manufacturing time constraints, and component selection constraints is shown in Fig. 3. This diagram displays the design point for a vehicle used in a wildlife searching and tracking mission, which is explored in more detail in Section V. In this mission, a baseline fixed wing UAV model similar to the one shown in Fig. 4 is used to search through a grid in a lawnmower pattern, and upon locating the target animal, to track and follow it. The searching phase involves following a predefined set of waypoints, while the tracking phase involves either following or orbiting about the animal, depending on its speed. These mission phases are explored further in Sections IV and V.

Figure 3 highlights some key considerations for the designer. The vehicle must use a motor that can generate sufficient power to meet the performance constraints. One of the constraint curves highlights the use of a motor which does not provide sufficient power to meet these constraints. Additionally, a battery with sufficient capacity to carry out the entire mission must be chosen. Another curve highlights the use of a motor/battery combination that meets point performance constraints, but does not have sufficient capacity. Typically, the battery size is not known when the constraint diagram is first generated, and selecting suitable components is an iterative process. Finally, the constraint diagram also shows how the use of multiple 3D printers for manufacturing can open up the space of feasible designs. The use of a single printer results in a minimum allowable *W/S* that is too large to meet the stall constraint, which defines a maximum allowable *W/S*. However, using an additional printer creates a feasible space. The following subsections explain the equations that govern the creation of these constraint curves.

A. Performance Constraints

Customer requirements can be converted into a number of performance-oriented constraints. These include: cruising speed, maximum rate of climb,turn requirements, takeoff distance, obstacle clearance, ceiling altitude and maximum stall speed. For fixed wing UAVs powered by batteries, *P/W* is used rather than *T/W*. Constraints are then represented with curves linking *P/W* and *W/S*. For all constraints, the curves define a region of the design space where any combination of *P/W* and *W/S* defines a feasible design. For instance, the ability to hand-launch the UAV is represented by an upper limit to the stall speed which in turn specifies a maximum allowable *W/S* for the UAV.

B. Manufacturing and Component Selection Constraints

Manufacturing and off-the-shelf electronic component selection constraints can also be captured within the constraint diagram. Sometimes, the customer needs the UAV solution within a set number of hours. This limits the time available to manufacture the various parts. Typically, if less time is available to manufacture the UAV, then the vehicle must be smaller or the number of manufacturing machines needs to be increased. The relationship between part manufacturing time (using additive manufacturing technology) and wing loading can be generated following the method of Justin et al. [6] and this yields a new constraint curve in the constraint diagram. Even though electronic components cannot be easily produced through rapid manufacturing techniques, commercially available off-the-shelf components can be integrated to yield an affordable vehicle design [9]. Once the electronic components are selected (motor, battery, ESC), the power available is essentially set and the relationship between electronic component selection and wing loading can then be derived. This yields another constraint curve in the constraint diagram. This last constraint, however, is different

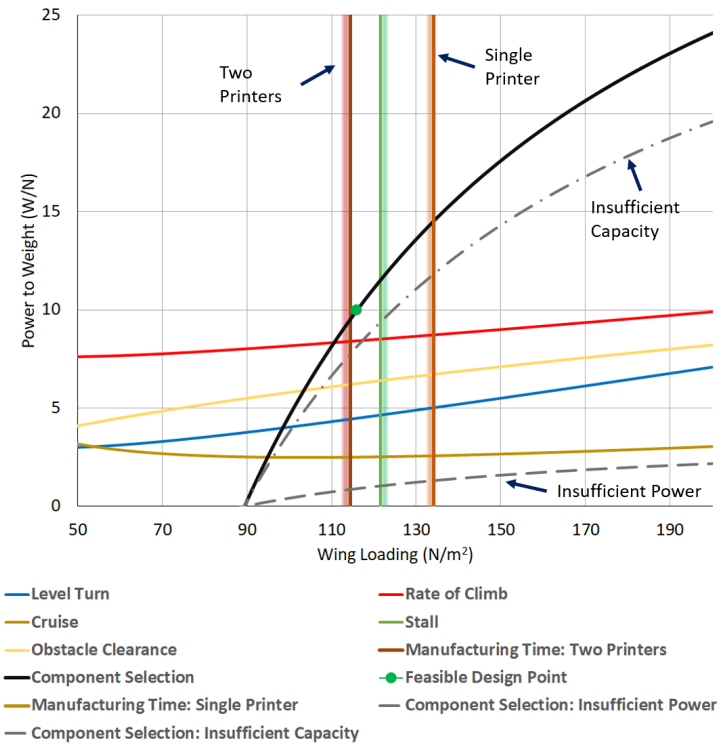

Fig. 3 Constraint diagram used for the wildlife searching and tracking mission.

from the others in that it does not define a region of the design space that is feasible but rather the locus of feasible wing loadings given the power available. This means that the design point needs to not only be chosen within the feasible design space as is traditionally done, but also on the component selection line [6]. These relationships are given by the following equations:

$$S = \frac{g(m_c + m_0)}{\frac{W}{S} - gm_1} \tag{1}$$

$$\frac{P}{W} = \frac{P}{g\left(m_c + m_0 + m_1\left(\frac{g(m_c+m_0)}{\frac{W}{S}-gm_1}\right)\right)} \tag{2}$$

$$\frac{W}{S} = gm_1 + \frac{t_1 g\,(m_c + m_0)}{t - t_0} \tag{3}$$

Where m_c is the assumed total mass for non-printed electronic components, and m_0, m_1, t_0 and t_1 are the regression coefficients of the linear UAV structural mass vs. wing area, and the UAV manufacturing time vs. wing area relationships. t is the total print time for all additively manufactured components of the vehicle. m_{str} is the structural mass of the vehicle, which is related to the total mass m of the vehicle as shown below:

$$m = m_{str} + m_c \tag{4}$$

$$m_{str} = m_0 + m_1 S \tag{5}$$

$$t = t_0 + t_1 S \tag{6}$$

The method initially proposed by Justin et al.[6] assumes an untapered wing and a linear relationship between print time and wing area in order to derive an expression for wing loading. It can however be further extended to account for wing taper. Let's consider a tapered wing made from multiple additively manufactured ribs. A rough sketch is provided in Fig. 5. Various parameters can be used to define the geometry of the wing, including the base chord length C_b, the

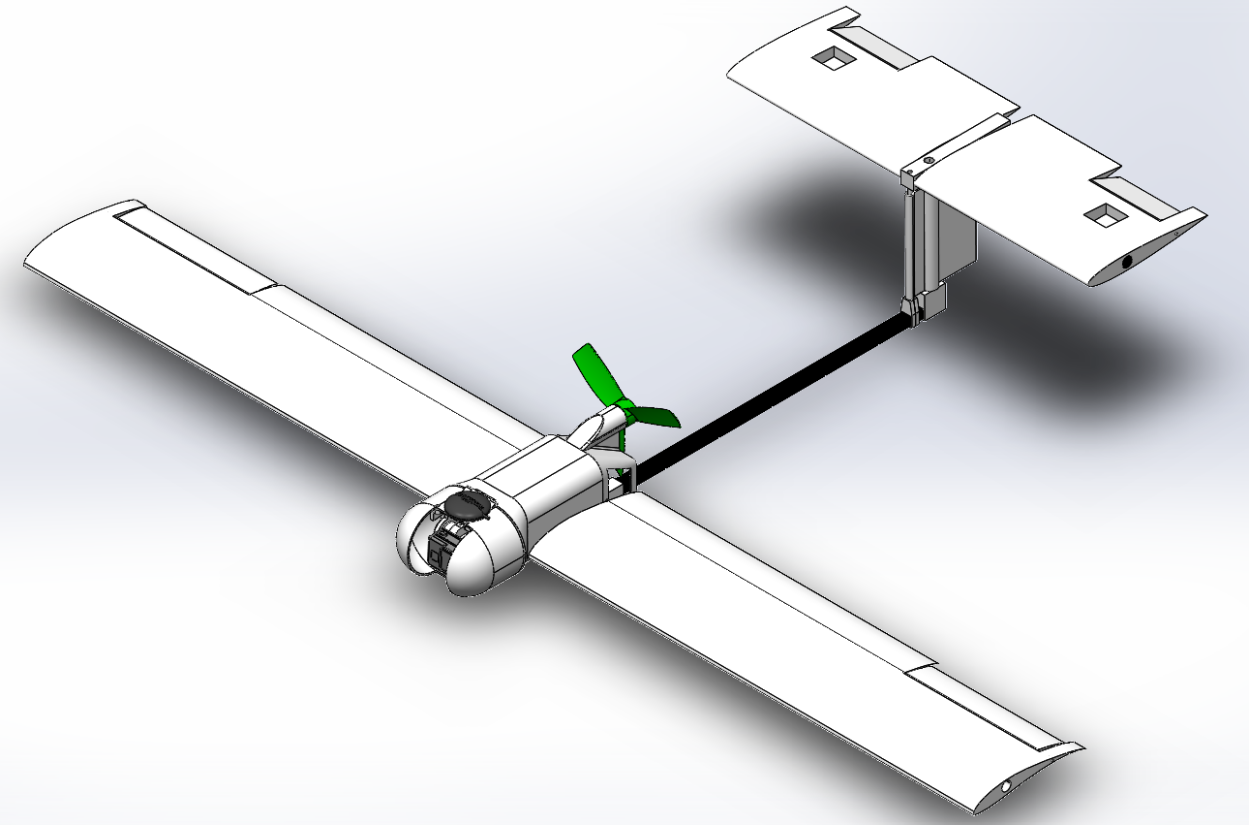

Fig. 4 Baseline UAV model used in constraint analysis.

half-span L, the rib spacing r, the number of ribs N in each half-wing, the distance a from the wing tip to the point at which chord length would be zero, and the taper ratio λ . The number of ribs is given by:

$$N = \frac{L}{r} + 1 \tag{7}$$

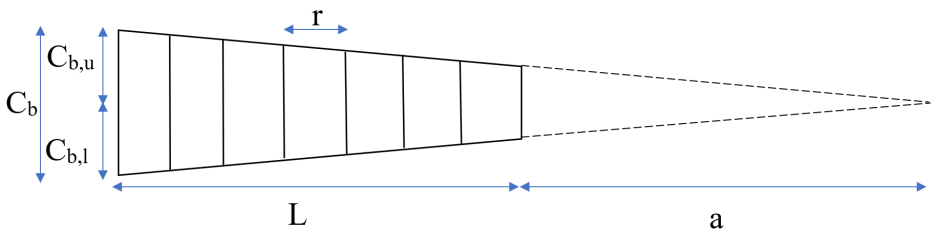

Fig. 5 Sketch of top view of a tapered wing with 3D printed ribs.

Using the properties of similar triangles, and Eq. (7) , the length of the ith rib is given by:

$$C_i = \left(1 - \frac{(1-\lambda)(i-1)}{\frac{L}{r}}\right) C_b \tag{8}$$

The relationship between the print time for the tapered wing and its area depends on the manner in which the wing is resized. It is logical to resize the wing by keeping the aspect ratio (AR) constant. This can be done by keeping

the number of ribs constant while changing the chord length and the spacing between ribs. The authors empirically derived that the print time for an individual wing rib is proportional to the square of its chord length. This is expected to be generally true, since print time is proportional to the square of a length metric. By summing print times for each individual rib, we can derive the print time T for the wing as:

$$T = KC_b^2 \sum_{i=1}^{N} \left(1 - \frac{(1-\lambda)(i-1)}{\frac{L}{r}}\right)^2 \tag{9}$$

where K is a proportionality constant. For the resizing method used, the taper ratio and number of ribs is constant as wing area changes. Using Eq. (7) this implies that the entire quantity being summed is constant with wing area. Eq. (9) can be replaced by:

$$T = K_2 C_b^2 \tag{10}$$

The base chord length can be expressed as:

$$C_b = \frac{S}{L(1+\lambda)} \tag{11}$$

This implies that:

$$T = K_2 \frac{S^2}{L^2(1+\lambda)^2} \tag{12}$$

For a constant AR, the quantity $\frac{L^2}{S}$ is constant. Therefore:

$$T = K_3 S \tag{13}$$

where K_3 is a constant coefficient. In other words, the print time for the wing increases linearly with wing area. Finally, this can be added to the print time for all other 3D printed components. For our vehicles, these components have either a fixed size, or a print time that varies linearly with wing area. Therefore, a final linear relationship is obtained for manufacturing time as a function of wing area, which can be used to re-derive Eq. (3).

It is also possible to derive an analytical solution when there is a quadratic relationship between manufacturing time and wing area. This is the case for tapered wings that are resized by keeping the span constant and changing the chord length. In this case, it can be assumed that the print time t is given by the following equation:

$$t = t_0 + \sum_{i=1}^{n} t_i f_i S \tag{14}$$

where t_i are constant coefficients and $f_i(S)$ are general functions of wing area S. Using empirical estimates or measurements of the print time for various wing areas, the coefficients can be found through a linear regression. For the specific case of a quadratic relationship between print time and wing area, an analytical expression for the wing loading can be developed. Using Eq. (1), the print time is given by:

$$t = t_0 + t_1 \left(\frac{g(m_c + m_0)}{\frac{W}{S} - gm_1}\right) + t_2 \left(\frac{g(m_c + m_0)}{\frac{W}{S} - gm_1}\right)^2 \tag{15}$$

Upon solving, the following expression is obtained:

$$\frac{W}{S} = gm_1 + \frac{2g(m_c + m_0)t_2}{\sqrt{4t_2(t - t_0) + t_1^2} \pm t_1} \tag{16}$$

Note that in this case, there are two potential solutions for the wing loading. The solution resulting in a higher wing loading is more constraining and is used in the constraint analysis.

The CURA software for Ultimaker 3D printers is used to obtain estimates of the structural mass and print time of all the 3D printed components of the vehicle. These are used to build up the coefficients of the UAV manufacturing time vs. wing area and total UAV mass vs. wing area relationships. Finally, these regression coefficients are used to obtain the component selection and manufacturing time constraint curves.

Note that in the preceding analysis, it is assumed that a single 3D printer is available. However, the use of multiple machines brings up a new optimization problem: how to print combinations of parts on available printers so as to reduce the total print time? This problem is a variant of the job shop scheduling problem [10] where many jobs (vehicle component prints) are allocated to one or more machines (3D printers) and the objective is to minimize the makespan (total print time of all components).

C. Print Scheduling

In the terminology of job shop scheduling, each part to be printed is referred to as a 'job', while each printer is a 'machine'. In this case, the problem is represented as $P_m||C_{max}$. P_m refers to the existence of m identical machines that can operate in parallel, while C_{max} refers to the objective of minimizing the makespan or total manufacturing time. The $P_m||C_{max}$ problem is NP-hard [11] and there is no solution which will always provide the true optimal schedule for the jobs. Instead, several heuristics have been developed for this problem, such as the Longest Processing Time first (LPT) rule. Following this rule, the m parts with the longest print times are assigned to the m available printers. After this, whenever a printer becomes available, the remaining part with the longest print time is assigned. The LPT rule gives a print schedule with a makespan which is at most 4/3 times the makespan of the unknown true optimal solution [11]. More accurately,

$$\frac{C_{max}\,(LPT)}{C_{max}\,(OPT)} < \left(\frac{4}{3} - \frac{1}{3m}\right) \tag{17}$$

where the Optimal Processing Time (OPT) refers to the true optimal solution.

An issue with using the LPT rule to assign parts to printers is that only one part can be printed at a time by any printer. This increases the need for human involvement in the process, since each part needs to be set up for printing and removed prior to printing a new part. Instead, multiple parts could be grouped together in a batch and printed simultaneously on a given printer. Another advantage of grouping parts in batches is that pre- and post-processing times for printing may be reduced. These include processes for which the time taken typically does not depend on the properties of the part, such as the heating of the print bed prior to the start of a print. However, there are disadvantages to part batching as well. When printing multiple parts, the printer head needs to travel more over the print bed, resulting in a slight increase in print times. Also, if a batch print were to fail, all the parts in the batch may fail to print. Finally, it is sometimes necessary to print certain parts with differing print settings (such as infill ratio). Typically, printers cannot handle parts with different settings within a single batch.

The problem of grouping jobs in batches to minimize the makespan has been discussed in the literature of job shop scheduling. However, the total processing time for the jobs in a batch is typically considered to be the time for the longest job in the batch [11]. This is not true for 3D printing, where the batch processing time is close to the sum of processing times for all parts in the batch. If pre and post processing times for printing (which are on the order of a few minutes) are ignored, the batch processing time is exactly equal to the sum of processing times for all constituent parts. On the other hand, if processing times are not excluded, batching may slightly reduce the makespan. However, this reduction is on the order of minutes, while, in the case of our vehicles, the makespan is on the order of several hours. Therefore, the authors concluded that the advantage of batching to reduce the makespan is insignificant. With no batching, the OPT time for a given set of parts tends to approach:

$$t_m = \frac{t}{m} \tag{18}$$

where t is the print time with a single printer and m is the number of printers. This equation is true if the printing load is evenly distributed among all printers. However, the print time when jobs are assigned using the LPT rule will be greater since jobs are not evenly distributed amongst the different machines. Also, Eq. (18) does not hold true as m is increased beyond a certain value. Indeed, there is a number of printers beyond which the total print time simply becomes the print time of the largest part, and it is impossible to decrease the print time any further. It is therefore clear that the relationship between print time and number of printers can be complex. It is nonetheless possible to account for this relationship within the manufacturing time constraint derived earlier. Eq. (16) can be generalized to account for the use of multiple printers. First, the print time can be written as:

$$t = t_0 + \sum_{i=1}^{k-2} t_i f_i(n) + t_{k-1} S + t_k S^2 \tag{19}$$

where $f_i(n)$ are general functions of the number of printers. On substituting Eq. (1) and solving for W/S, we obtain:

$$\frac{W}{S} = g m_1 + \frac{2g(m_c + m_0)t_k}{\sqrt{4t_k\left(t - t_0 - \sum_{i=1}^{k-2} t_i f_i(n)\right) + t_{k-1}^2} \pm t_{k-1}} \tag{20}$$

The change in manufacturing time as a function of both wing loading and number of printers, is investigated for one of our baseline vehicles. First, total print times for various wing areas are estimated using the CURA 3D printing software.

Table 1 Selected print times for baseline vehicle

Model Print Times	Wing Area: 0.125 m^2		Wing Area: 0.15 m^2		Wing Area: 0.175 m^2	
Part	Time (min)	Quantity	Time (min)	Quantity	Time (min)	Quantity
Selig Flap	35	2	49	2	64	2
Selig Main Wing	493	2	634	2	918	2
Nosecone	235	1	235	1	238	1
Horizontal Stabilizer Slot	123	1	123	1	123	1
NACA Flap (1)	48	2	62	2	82	2
NACA Flap (2)	161	2	265	2	341	2
Fuselage	393	1	393	1	393	1
Vertical Stabilizer Slot (Back)	34	1	34	1	34	1
Vertical Stabilizer Slot	7	2	7	2	7	2
Vertical Stabilizer	215	1	251	1	286	1

Table 2 Selected total print times for baseline vehicle

	Wing Area: 0.125 m^2	Wing Area: 0.15 m^2	Wing Area: 0.175 m^2
Number of Printers	Total Print Time (min)	Total Print Time (min)	Total Print Time (min)
1	2,488	3,070	3,898
2	1,246	1,544	1,951
3	838	1038	1,302
4	624	779	982
5	510	634	918
6	493	634	918
7	493	634	918
8	493	634	918
9	493	634	918
10	493	634	918

Table 1 provides a sample of the print times found for all printed parts for three wing areas. Next, a MATLAB script is used to assign parts to m printers (m ranging from 1 to 10) for the three wing areas using the LPT rule, and to estimate the total print time. Table 2 shows a sample of the results.

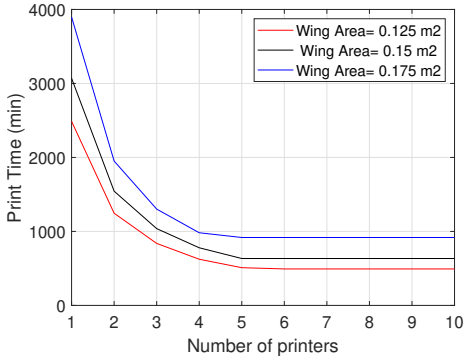

Fig. 6 Total print times as a function of number of printers at three wing areas.

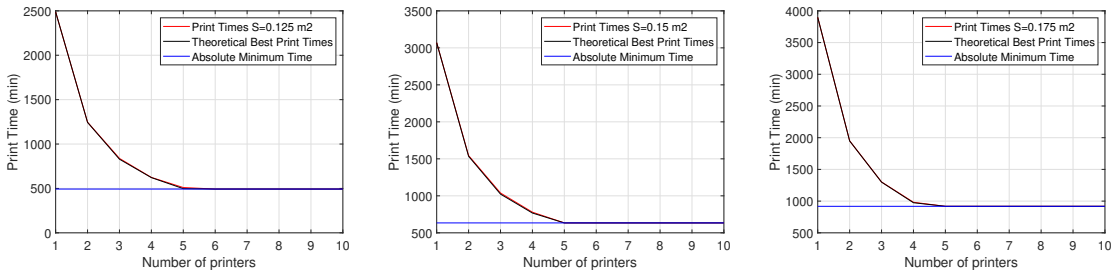

(a) **(b)** **(c)**

Fig. 7 Comparison of LPT print times with theoretical minimum times.

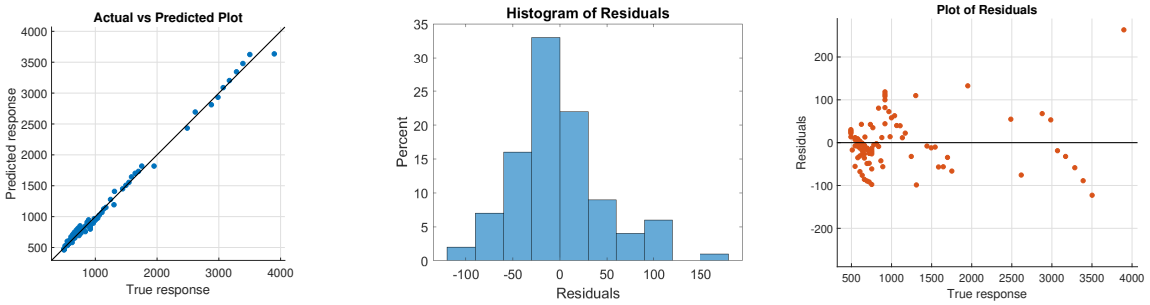

(a) **(b)** **(c)**

Fig. 8 Goodness of fit plots for manufacturing time regression.

The results shown in Table 2 are shown graphically in Fig. 6. For different wing areas, the relationship between the print time and number of printers is similar. The figure also displays the flattening of the curve once a critical number of printers is used, corresponding to the absolute minimum print time. Figure 7 further analyzes these print times by comparing them to the theoretical best print times i.e. an evenly distributed print load as shown in Eq. (18). As the figure shows, the difference between the two sets of print times is very small, and is in fact never greater than 3%. This is because there is a large number of parts with small print times, which makes it easier to distribute the load almost evenly among the machines using the LPT rule. The absolute minimum print time in Fig. 6 is the print time for the largest part. Based on these results, a multivariate linear regression is performed using MATLAB to capture manufacturing time as a function of S, $\frac{1}{m}$ and $\frac{1}{m^2}$, including the main effects as well as interactions. An R^2 value of 0.99 was achieved. Figure 8 shows some key goodness-of-fit plots for the regression. The actual vs predicted plot shows a very accurate fit. The error distribution is nearly normal, although slightly offset from a mean of zero. The residuals seem randomly distributed, though there is some clumping for lower response values. However, there are also far more data points at lower response values than at higher ones, which can be seen in the actual vs predicted plot.

III. Design Point Selection and Manufacturing

Once the design space has been explored, a single point within the feasible design space is selected and used to resize the baseline UAV model by either increasing or decreasing the wing surface. For a given set of initially chosen electronic components, the selected design point fully defines the vehicle design attributes. Indeed, since the available power is known from the selection of the motor and battery, the structural weight of the UAV can be found from the Power to Weight at the design point. The wing area can then be found using the vehicle weight and the wing loading. The design properties such as aspect ratio and taper ratio that were previously used as an input to derive the manufacturing time and component selection curves, can now be used to properly size the vehicle. Once the vehicle weight is found, an iterative process is used in order to size the battery and define the final set of electronic components. For each phase of the mission, the required P/W from the corresponding performance constraint can be linked to a required battery capacity.

The total capacity is then found from the following equation:

$$Capacity = \frac{W}{0.8} V \sum_{i=1}^{c} (P/W)_i \, t_i \tag{21}$$

For each mission phase, the power required is used to calculate the corresponding battery capacity using the time t_i spent in the phase, the vehicle weight W and the battery voltage V. The total capacity is found and divided by 0.8 to ensure that the full capacity of the battery is never used. The minimum capacity required is compared to the total capacity available from the currently chosen battery component. If the capacity is insufficient, a new battery component can be selected, which may change the power available and result in a new vehicle weight. A new design point can be chosen, Eq. (21) can be used again and the process is repeated until a final set of components is established.

Once the vehicle is sized, it is ready to be manufactured and assembled. For our vehicles, all structural parts are manufactured using additive manufacturing. Parts are designed to have a minimal print time using several techniques, such as incorporating holes or shells to minimize material, and minimizing the need for support material by eliminating overhangs. All parts can be auto-oriented into an optimal position for reducing print time, using Meshmixer [12], a freely available software for working with 3D printable parts. A Python script is written to extract 3D part files, automatically orient them for minimal print time, and save them in a ready-to-print configuration. A script is written to assign parts to available printers in accordance with the LPT rule. Finally, the printed parts can be assembled along with the previously selected electronic components to obtain a ready-to-fly vehicle.

IV. Mission Simulation

Simulating the mission can provide helpful insights about the performance of the UAV and allows the designer to create a detailed mission plan that exploits the vehicle's design properties. A low-fidelity simulation environment is created using the Simulink UAV library. This includes a fixed-wing UAV model as well as Waypoint Follower and Orbit Follower tools. First, a method is developed to link design constraints to the behavior of the simulated vehicle. The Simulink UAV library uses the L1 guidance algorithm [13] for waypoint following, which is commonly used on UAV flight controllers [14]. Therefore, it is useful to incorporate vehicle constraints into the L1 parameters. In L1 guidance, a set of waypoints is used as input to the UAV flight controller. When the vehicle is in-between waypoints, it "looks ahead" by a distance L along the projected path joining the previous and subsequent waypoints. A roll angle is commanded so that the vehicle can align itself with this path segment. The vehicle is assumed to operate in the coordinated turn condition, and therefore the heading angle is directly linked to the roll angle. The pitch angle is determined based on the current altitude and the altitude of the next waypoint, while the airspeed is controlled by the user. Once the vehicle is close enough to a waypoint, it enters a "transition zone" defined as a sphere of radius R' where the vehicle begins to look ahead to the next waypoint. The optimal value for the "look ahead" distance L is linked to the minimum turn radius achievable by the vehicle, and therefore it can be linked to the maximum allowed load factor and the cruising speed.

$$\phi_{max} = cos^{-1} \frac{1}{\delta} \tag{22}$$

Here δ is the maximum load factor and ϕ_{max} is the maximum roll angle. Then the minimum turn radius R is:

$$R = \frac{V_g^2}{g tan(\phi_{max})} \tag{23}$$

Here V_g is the cruising speed and g is gravitational acceleration. Finally, L is found to be:

$$R' = R \sqrt{\frac{1 + cos\theta}{1 - cos\theta}} \tag{24}$$

$$L = \sqrt{2R'^2 (1 - cos\theta)} \tag{25}$$

Here θ is the angle between two consecutive waypoint segments and R' is the transition radius. We can now adapt the simulation behavior to match the vehicle design properties.

The simulation environment can also be used to plan a mission, allowing the designer to link design properties to the mission profile. This creates a loop in the design process, as seen in Fig. 2. Mission planning can be carried out

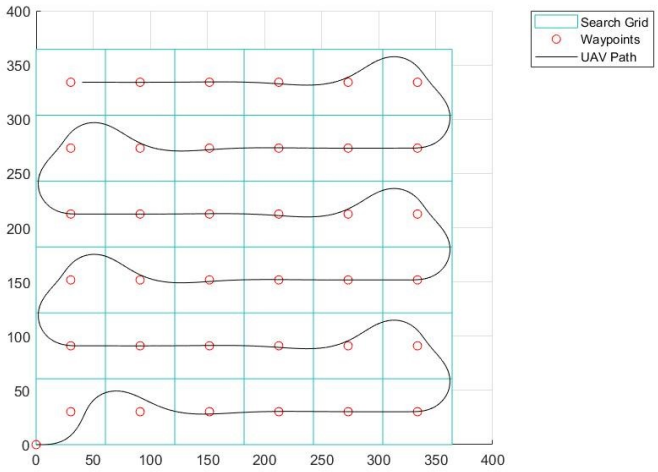

(a)

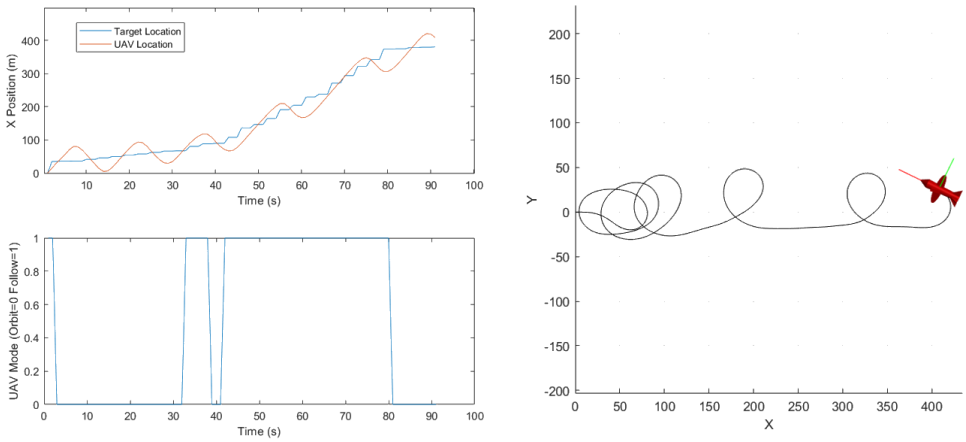

(b)

Fig. 9 Results of target search simulation run (UAV size not to scale) and visualization of search approach.

for a given model, which in turn can be used to derive mission requirements that will size the model. For instance, a mission plan for the wildlife tracking use case is generated and includes two phases: a searching phase and a tracking phase. For the searching aspect of the mission, a simple lawnmower/complete coverage search approach is used. The UAV searches a given area by sweeping through a search grid made of square cells. The cell size is set to twice the minimum turn radius of the vehicle, which is itself linked to the maximum load factor as shown in Eq. (22) and Eq. (23). Therefore, when the UAV exits one row of the grid, it starts a 180 degree turn with the minimum radius to enter the next row of the grid. In this way, the manner in which the mission is executed can be linked to the design properties of the vehicle. When the vehicle enters the same cell as the target, it is assumed to have located the target. For the tracking aspect of the mission, the target is assumed to move in a 2D environment with no obstacles, at a given average speed disturbed using a serially correlated noise component. The UAV will either follow the target or orbit around it, depending on whether the target is moving faster than the stall speed defined for the vehicle model. The orbit radius is specified by the minimum turn radius for the vehicle. Figure 9a shows a visualization of the searching approach. Figure 9b shows the results of a target tracking simulation with the target moving in the positive X-direction, and the path followed by the UAV in the XY plane.

V. Use Case

The design process developed in the previous sections is demonstrated for a particular use case: locating, tracking, and following wildlife to identify threats. Due to poaching activity, it is not possible to publish research containing data about the actual whereabouts of black rhinos. Therefore, data for a commonly found species, which is not currently at risk, is used to demonstrate the use of the proposed framework. The data is obtained from a study done on wild olive baboons at Mpala Research Center in Kenya [15][16]. Preprocessing was done on the data to convert it from latitude/longitude to position in meters using an equirectangular projection. Figure 10 displays the converted data for a single animal over a 12 hour period.

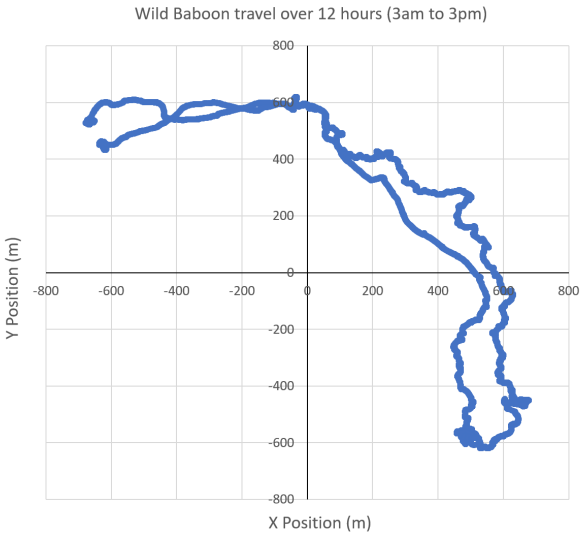

Fig. 10 Movement data for a wild olive baboon over a 12 hour period.

A design mission is then created for the UAV. It involves a takeoff and climb to the cruise altitude, a grid search pattern to search the region of interest and locate the animals, some loitering in the vicinity of the animals in order to identify potential poaching activity, and finally a return to the home base. An iterative process is used to define the constraints and size the vehicle. First, initial assumptions are made regarding the specifications and attributes of the vehicle and its components. For instance, the vehicle uses the S1210 airfoil, for which a $C_{L,max}$ value of 1.8 at low speeds has been calculated [17]. A design point is selected and Eq. (2) is used to obtain the corresponding vehicle weight. Eq. (21) is then used to determine the minimum required battery capacity in units of Ah. The final design mission is constructed as follows:

- Take off and clear an obstacle at a height of 25m within 100m
- Climb at 3.5 m/s to an altitude of 50 m
- Cruise a distance of 1km to the search region
- Conduct a lawnmower-pattern search through the region with a search grid size of 1600mx1600m
- Locate the target and track it for 20 min in orbit following mode
- Return to base
- Achieve a stall speed of 10.5 m/s
- Provide a turn-key solution under 48 hrs using two 3D printers

Figure 11 shows a sketch of the design mission, while the corresponding constraint diagram for the final design point is shown in Fig. 3. In Fig. 11, the brown square represents a 1600mx1600m grid containing the animal tracks from Fig. 10. The vehicle is assumed to locate an animal in the upper right corner of the search grid. Using Eq. (1), the wing area for the design vehicle was found and used to resize the CAD model. The print time and mass regressions were used to calculate the time required to manufacture the UAV and the total mass. Some of the key parameters defining the chosen design are summarized in Table 3.

A simulation is run for the searching and tracking portion of the mission, with the design mission parameters used to set corresponding simulation parameters. In order to reduce the simulation run time, the origin of the movement data was shifted so that the UAV would encounter the target within the first 90 seconds. As noted earlier, the simulation could be adapted to the performance constraints of the vehicle. Parameters such as lookahead distance and maximum

Table 3 Key parameters for design vehicle.

Vehicle Mass (kg)	Wing Area (m^2)	Manufacturing Time (hrs)	Available Power (W)	Required Capacity (mAh)
2.54	0.207	38.0	278	1990

allowable roll angle were set using an assumed load factor constraint of 1.5. However, this constraint was not used to define the size of the cells in the search grid. Instead, these had been predefined by the design mission. Figure 12 displays the results of the simulation. In Fig. 12a and Fig. 12b, the vehicle is in searching mode (shown in red), and searches through a grid with cells of size 200mx200m in a lawnmower pattern while the target (in blue) moves through the search region. Note that the size of the complete search grid was reduced for the simulation, though the cell size was kept the same. Figure 12c shows the UAV in tracking mode (shown in green) after locating the target. Since the speed of the target is well below the UAV stall speed, the UAV remains in orbit following mode and spirals around the target location.

This simple simulation environment can be used in parallel with the constraint analysis in order to test different design missions. Parameters such as search grid size and the UAV guidance variables can be changed in the simulation to improve searching or tracking characteristics. These changes will define a new mission, and the constraint analysis can be used to verify that the energy requirements for the mission do not exceed the available capacity.

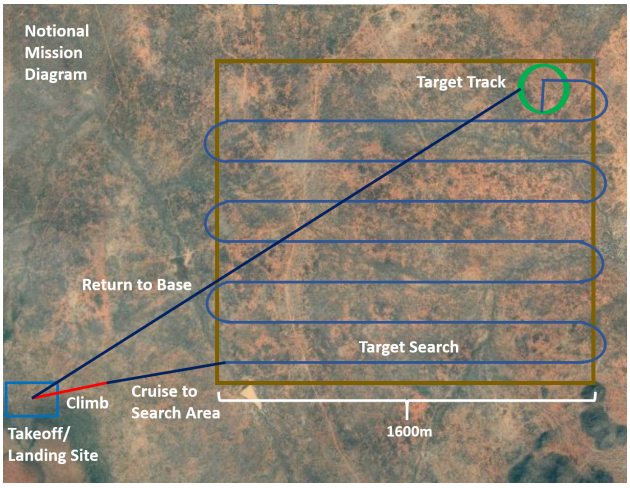

Fig. 11 Diagram of design mission.

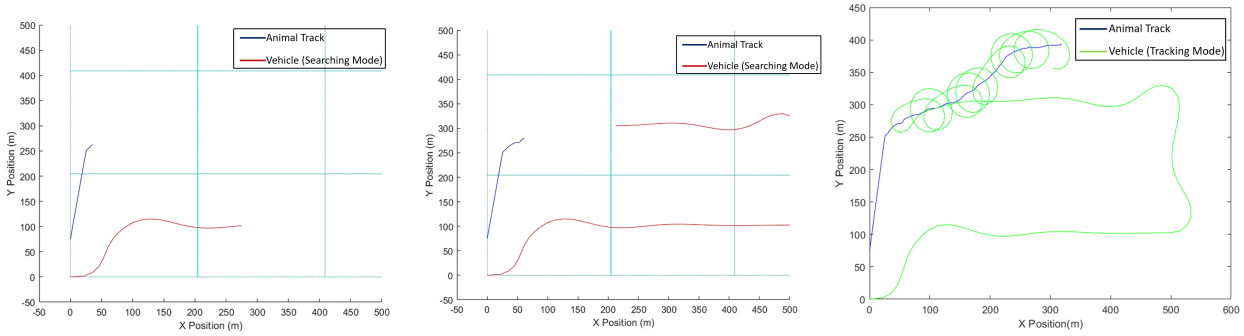

(a) **(b)** **(c)**

Fig. 12 Results of target search simulation run using movement data.

VI. Conclusion

This paper documents a parametric design process for an on-demand fixed wing UAV leveraging advances in additive manufacturing technologies to create an attritable product tailor-made to some mission specification. The design process consists of several coupled multidisciplinary subproblems that can be linked together by specifying mission parameters and design constraints. This allows every aspect of the design process to be adapted towards creating a vehicle for a specific mission. Design space exploration is performed by capturing performance, manufacturing and component availability requirements as constraints of Power to Weight vs wing loading. These constraints also account for the geometry of the vehicle model and the use of multiple 3D printers. From the constraint analysis, an optimal design is selected, and the baseline vehicle is sized to meet the requirements. Mission simulations is used to construct a mission that fits the constraints of the physical vehicle. This approach is used to simulate a target searching and tracking mission. Finally, a demonstration of the design, sizing and simulation process is presented for an example vehicle derived for a wildlife tracking use case.

Several avenues of future work can be identified. First, flight tests need to be performed on a manufactured vehicle in order to verify and validate the flight characteristics of the vehicle for different wing sizes and combinations of motors and batteries. Multiple vehicles sized for different missions can also be flown to assess the change in flight behavior when optimizing for different missions. The parametric design process can also be extended to the flight controllers. Commonly used autopilot platforms such as the PX4 or ArduPilot make use of more advanced forms of the L1 guidance algorithm presented in this paper [14]. Therefore, flight controllers could be tuned so that the vehicle behavior is optimized for its mission. Finally, the accuracy of the manufacturing time estimates could be further improved by accounting for the assembly time of the vehicle once the production of all the structural parts of the vehicle is complete.

Acknowledgments

The authors would like to thank Michael Gamarnik and Tristan Huang for their help with designing the CAD models for the baseline vehicles and conducting research on finding suitable electronic components.

References

[1] International Rhino Foundation, "Black Rhino," , Retrieved November 2020. URL https://rhinos.org/about-rhinos/rhino-species/black-rhino/.

[2] International Union for Conservation of Nature, "Conservation efforts bring cautious hope for African rhinos," , March 2020. URL https://www.iucn.org/news/species/202003/conservation-efforts-bring-cautious-hope-african-rhinos-iucn-red-list.

[3] Nuwer, R., "In an Effort to Stop Poaching, Namibia Will Remove All of Its Rhinos' Horns," , 2014. URL https://www.smithsonianmag.com/smart-news/effort-stop-poaching-namibia-will-remove-all-its-rhinos-horns-180953052/.

[4] Calkin, J., "Rhinos under 24-hour armed guard," , September 2012. URL https://www.telegraph.co.uk/news/earth/wildlife/9525512/Rhinos-under-24-hour-armed-guard.html.

[5] Mangewa, L., Ndakidem, P., and Munishi, L., "Integrating UAV Technology in an Ecological Monitoring System for Community Wildlife Management Areas in Tanzania," *Sustainability*, Vol. 11, No. 21, 2019, pp. 1–17. https://doi.org/10.3390/su11216116.

[6] Justin, C., Ramamurthy, A., Beals, N., Spero, E., and Mavris, D., "On-Demand Small UAS Architecture Selection and Rapid Manufacturing using a Model-Based Systems Engineering Approach," 2018.

[7] Petnga, L., "Constraint-driven Design Specification for Small Unmanned Aircraft Systems," 2018. https://doi.org/10.2514/6.2018-1214.

[8] Mattingly, J., Heiser, W. H., and Pratt, D. T., *Aircraft Engine Design*, AIAA, Reston, VA, 2002.

[9] Mangum, P., Fisher, Z., Cooksey, K. D., Mavris, D., Spero, E., and Gerdes, J. W., "An Automated Approach to the Design of Small Aerial Systems Using Rapid Manufacturing," *ASME 2015 International Design Engineering Technical Conferences and Computers and Information in Engineering Conference*, Vol. 2B, ASME, Boston, MA, 2015. https://doi.org/10.1115/DETC2015-47786.

[10] Lenstra, J., *Job Shop Scheduling. In:Combinatorial Optimization*, Springer Berlin, Heidelberg, 1992, NATO ASI Series (Series F: Computer and Systems Sciences), Vol. 82.

[11] Pinedo, M. L., *Scheduling Theory, Algorithms and Systems*, 4th ed., Springer, New York, 2011, pp. 112,113.

[12] Schmidt, R., and Ratto, M., "Design Tools for the Rest of Us: Maker Hardware Requires Maker Software," 2013. URL https://damassets.autodesk.net/content/dam/autodesk/www/autodesk-reasearch/Publications/pdf/design-tools-for-the.pdf.

[13] Park, S., Deyst, J., and How, J., "A New Nonlinear Guidance Logic for Trajectory Tracking," 2004.

[14] Stastny, T., "L1 guidance logic extension for small UAVs: handling high winds and small loiter radii," *CoRR*, Vol. abs/1804.04209, 2018. URL http://arxiv.org/abs/1804.04209.

[15] Strandburg-Peshkin, A., Farine, D. R., Couzin, I. D., and Crofoot, M. C., "Shared decision-making drives collective movement in wild baboons," *Science*, Vol. 348, No. 6241, 2015, pp. 1358–1361. https://doi.org/10.1126/science.aaa5099, URL https://science.sciencemag.org/content/348/6241/1358.

[16] Crofoot, M., Kays, R., and Wikelski, M., "Data from: Shared decision-making drives collective movement in wild baboons," , 2015. https://doi.org/doi:10.5441/001/1.kn0816jn, URL http://dx.doi.org/10.5441/001/1.kn0816jn.

[17] Selig, M., Guglielmo, J., Broeren, A., and Giguère, P., *Summary of Low-Speed Airfoil Data*, SoarTech Publications, Virginia Beach, VA, 1995, Vol. 1, p. 48.